# A Study of Dissipation Operators for the Euler Equations and a Three-dimensional Channel Flow

Pelle Olsson and S. Lennart Jonsson

YALEU/DCS/TR-732
September 1989

To appear in the Proceedings of Supercomputing 1989

# A Study of Dissipation Operators for the Euler Equations and a Three-dimensional Channel Flow.

Pelle Olsson
Department of Scientific Computing
Uppsala University
Uppsala, Sweden
and
Department of Computer Science
Yale University
New Haven, CT 06520

S Lennart Johnsson
Thinking Machines Corp.
245 First Street
Cambridge, MA 02142
and
Departments of Computer Science
and Electrical Engineering
Yale University
New Haven, CT 06520

## Abstract

Explicit methods for the solution of fluid flow problems are of considerable interest in supercomputing. These methods parallelize well. The treatment of the boundaries is of particular interest both with respect to the numeric behavior of the solution, and the computational efficiency. We have solved the three-dimensional Euler equations for a twisted channel using second-order, centered difference operators, and a three stage Runge-Kutta method for the integration. Three different fourth-order dissipation operators were studied for numeric stabilization: one positive definite, [8], one positive semidefinite, [3], and one indefinite. The operators only differ in the treatment of the boundary. For computational efficiency all dissipation operators were designed with a constant bandwidth in matrix representation, with the bandwidth determined by the operator in the interior. The positive definite dissipation operator results in a significant growth in entropy close to the channel walls. The other operators maintain constant entropy.

Several different implementations of the semidefinite operator obtained through factoring of the operator were also studied. We show the difference both in convergence rate and robustness for the different dissipation operators, and the factorizations of the operator due to Eriksson. For the simulations in this study one of the factorizations of the semidefinite operator required 70 - 90% of the number of iterations required by the positive definite operator. The indefinite operator was sensitive to perturbations in the inflow boundary conditions. The simulations were performed on a 8,192 processor Connection Machine system model CM–2. Full processor utilization was achieved, and a performance of 135 Mflops/s in single precision was obtained. A performance of 1.1 Gflops/s for a fully configured system with 65,536 processors was demonstrated.

## 1 Introduction

Explicit methods are of considerable interest in supercomputing. Supercomputer architectures are parallel architectures. Some of todays supercomputers have thousands to tens of thousands of processors. The next generation supercomputers with a performance of a trillion floating-point operations per second are all expected to have thousands to tens of thousands of processors [5]. Explicit methods parallelize well, but depend critically on the use of artificial viscosity to stabilize the numerical scheme. The treatment of the boundaries is important numerically and computationally. With a lower order difference operator at the boundary, the boundary operator can be designed to contain a subset of the points of the operator in the interior. The complete set of stencils for the interior and the boundary can be represented as a matrix of constant bandwidth. Such a collection of operators results in good load balance and communication efficiency on parallel computers. Several methods for the introduction of artificial viscosity have been proposed, with the one proposed by Eriksson [3] being one of the most common. It is positive semidefinite. We have also included a positive definite [8] and an indefinite operator in our study. We demonstrate how different implementations of the same dissipation operator affect the robustness of an operator. We also demonstrate the importance of a conservative dissipation operator on the flow in a twisted channel with grids of up to 65,536 points. The simulations were carried out on Connection Machine systems, model CM–2. Most of the results were obtained on a 8,192 processor configuration. A performance of 1.1 Gflops/s was demonstrated on a 65,536 processor system. The data parallel implementation is described in [6].

The Euler equations are stated in the next section. The boundary conditions are extensively discussed in [7]. The artificial viscosity is treated in section 3, and the computational results are presented in section 4. Summary and conclusions are given in section 5.

# 2 The Mathematical Model

Our simulations are based on the conservative formulation of the Euler equations in order to allow for shock capturing. The conservative Euler equations are

$$\frac{\partial \mathbf{q}}{\partial \tau} = \frac{\partial \mathbf{F}}{\partial \xi} + \frac{\partial \mathbf{G}}{\partial \eta} + \frac{\partial \mathbf{H}}{\partial \zeta}, \tag{1}$$

where the variable vector $\mathbf{q}$ is given by

$$\mathbf{q} = |\mathbf{J}|^{-1} \begin{pmatrix} \rho \\ \rho u \\ \rho v \\ \rho w \\ e \end{pmatrix}. \tag{2}$$

The components of the variable vector $\mathbf{q}$ have the following meaning:

| | |
|---|---|
| $\rho$ | density |
| $\rho u$ | x-component of linear momentum |
| $\rho v$ | y-component of linear momentum |
| $\rho w$ | z-component of linear momentum |
| $e$ | total energy. |

Here $\tau$,$\xi$, $\eta$ and $\zeta$ denote the variables in the computational domain. The transformation between the computational domain and the physical domain represented by $t$, $x$, $y$, and $z$ is assumed to be continuously differentiable and non-singular:

$$\begin{cases} \tau &= t \\ \xi &= \xi(t,x,y,z) \\ \eta &= \eta(t,x,y,z) \\ \zeta &= \zeta(t,x,y,z) \end{cases}.$$

The Jacobian matrix $\mathbf{J}$ is defined by

$$\mathbf{J} = \begin{pmatrix} 1 & 0 & 0 & 0 \\ \xi_t & \xi_x & \xi_y & \xi_z \\ \eta_t & \eta_x & \eta_y & \eta_z \\ \zeta_t & \zeta_x & \zeta_y & \zeta_z \end{pmatrix}. \tag{3}$$

The subscripts denote partial differentiation. The functional determinant of the Jacobian matrix, $|\mathbf{J}|$, corresponds to the reciprocal cell volume:

$$|\mathbf{J}| = \det \begin{pmatrix} 1 & 0 & 0 & 0 \\ \xi_t & \xi_x & \xi_y & \xi_z \\ \eta_t & \eta_x & \eta_y & \eta_z \\ \zeta_t & \zeta_x & \zeta_y & \zeta_z \end{pmatrix} = \det \begin{pmatrix} (\nabla\xi)^T \\ (\nabla\eta)^T \\ (\nabla\zeta)^T \end{pmatrix}, \tag{4}$$

where

$$\nabla^T = \begin{pmatrix} \frac{\partial}{\partial x} & \frac{\partial}{\partial y} & \frac{\partial}{\partial z} \end{pmatrix}. \tag{5}$$

The flux vectors $\mathbf{F}$, $\mathbf{G}$ and $\mathbf{H}$ have the following components (inviscid case):

$$\mathbf{F} = -U\mathbf{q} - p|\mathbf{J}|^{-1} \begin{pmatrix} 0 \\ \nabla\xi \\ U - \xi_t \end{pmatrix} \tag{6}$$

$$\mathbf{G} = -V\mathbf{q} - p|\mathbf{J}|^{-1} \begin{pmatrix} 0 \\ \nabla\eta \\ V - \eta_t \end{pmatrix} \tag{7}$$

$$\mathbf{H} = -W\mathbf{q} - p|\mathbf{J}|^{-1} \begin{pmatrix} 0 \\ \nabla\zeta \\ W - \zeta_t \end{pmatrix}, \tag{8}$$

and $U$, $V$ and $W$ are the contravariant velocity components:

$$\begin{pmatrix} U \\ V \\ W \end{pmatrix} = \mathbf{J}' \begin{pmatrix} 1 \\ u \\ v \\ w \end{pmatrix}. \tag{9}$$

$\mathbf{J}'$ denotes the $3 \times 4$ matrix which is obtained by deleting the first row of $\mathbf{J}$. In the flux vector expressions, $p$ denotes the pressure, which is related to the total energy according to

$$p = (\gamma - 1)(e - \frac{\rho}{2}(u^2 + v^2 + w^2)), \tag{10}$$

where $\gamma$ is the ratio of the specific heats $c_p/c_v$. We assume that $\gamma$ is a constant having the value 1.4.

In [7] the in- and outflow boundary conditions are considered in detail. At each point on the in/outflow boundaries, $\zeta = 0$ and $\zeta = N_\zeta$, the values of $\rho, w$ and $p$ are determined by solving a 3 by 3 system of equations

$$\begin{pmatrix} a_0^2 & 0 & -1 \\ 0 & \rho_0 a_0 & 1 \\ 0 & -\rho_0 a_0 & 1 \end{pmatrix} \begin{pmatrix} \rho \\ w \\ p \end{pmatrix} \equiv \begin{pmatrix} \phi_3 \\ \phi_4 \\ \phi_5 \end{pmatrix}. \tag{11}$$

The variables $\phi_3, \phi_4$ and $\phi_5$, defined by (11), are the characteristic variables. Hence, the above formula is always used to compute the *linearized* characteristic variables. To have a well posed problem input data must be properly treated. The following procedure leads to a well posed problem [7].

- Subsonic inflow: Compute $\phi_3$ and $\phi_4$ from the reference level $\rho_0, w_0$ and $p_0$ at the inflow. The variable $\phi_5$ is computed using the flow variables $\rho, w$ and $p$.
- Subsonic outflow: Compute $\phi_5$ from the reference level $\rho_0, w_0$ and $p_0$ at the outflow. The variables $\phi_3$ and $\phi_4$ are computed using the flow variables $\rho, w$ and $p$.
- Supersonic inflow: Compute $\phi_3, \phi_4$ and $\phi_5$ from the reference level $\rho_0, w_0$ and $p_0$ at the inflow.
- Supersonic outflow: Compute $\phi_3, \phi_4$ and $\phi_5$ from the flow variables $\rho, w$ and $p$.

The characteristic thus computed, equation (11) is solved for $\rho, w$ and $p$. It should be noted that there is no need for solving (11) in case of supersonic in/outflow. Finally, $u = v = 0$ at the inflow for both subsonic and supersonic flow.

## 2.1 Symmetry Properties

We assume a time independent geometry. Since the channel is a twisted parallelepiped, it is natural to assume that the solution possesses some kind of symmetry properties. The coordinate transformation

$$\begin{cases} x(\xi,\eta,\zeta) &= \xi\cos(\omega\zeta) - \eta\sin(\omega\zeta) \\ y(\xi,\eta,\zeta) &= \xi\sin(\omega\zeta) + \eta\cos(\omega\zeta) \\ z(\xi,\eta,\zeta) &= \zeta \end{cases} \tag{12}$$

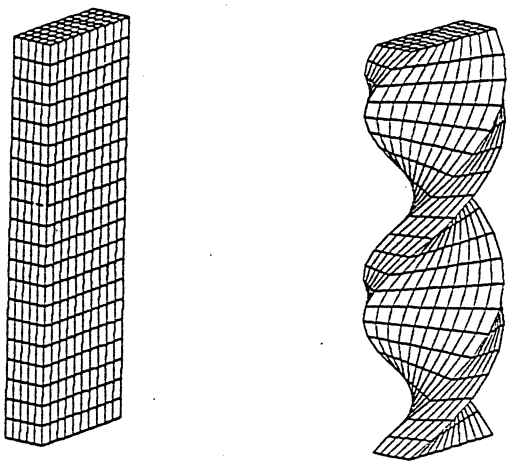

Figure 1: Computational and Physical Domain

describes a twisted parallelepiped with a twisting factor of $\omega$. This gives the flux vectors

$$\mathbf{F} = -\begin{pmatrix} \rho U \\ \rho u U + p\cos(\omega\zeta) \\ \rho v U + p\sin(\omega\zeta) \\ \rho w U + p\omega\eta \\ (e+p)U \end{pmatrix} \tag{13}$$

$$\mathbf{G} = -\begin{pmatrix} \rho V \\ \rho u V - p\sin(\omega\zeta) \\ \rho v V + p\cos(\omega\zeta) \\ \rho w V - p\omega\xi \\ (e+p)V \end{pmatrix} \tag{14}$$

$$\mathbf{H} = -\begin{pmatrix} \rho W \\ \rho u W \\ \rho v W \\ \rho w W + p \\ (e+p)W \end{pmatrix}. \tag{15}$$

Replacing $\xi$ and $\eta$ by $-\xi$ and $-\eta$ in equation (1) yields

$$\frac{\partial \mathbf{q}}{\partial \tau} = -\frac{\partial \mathbf{F}}{\partial \xi} - \frac{\partial \mathbf{G}}{\partial \eta} + \frac{\partial \mathbf{H}}{\partial \zeta}, \tag{16}$$

where the flux vectors are defined by (13), (14) and (15). All variables are evaluated at the point $(-\xi,-\eta,\zeta)$. Define

$$\begin{cases} \bar{u}(\xi,\eta,\zeta) &= -u(-\xi,-\eta,\zeta) \\ \bar{v}(\xi,\eta,\zeta) &= -v(-\xi,-\eta,\zeta) \\ \bar{w}(\xi,\eta,\zeta) &= w(-\xi,-\eta,\zeta) \end{cases}. \tag{17}$$

Using this definition and equations (9) and (12) it follows that

$$\begin{cases} U(-\xi,-\eta,\zeta) &= -\bar{U}(\xi,\eta,\zeta) \\ V(-\xi,-\eta,\zeta) &= -\bar{V}(\xi,\eta,\zeta) \\ W(-\xi,-\eta,\zeta) &= \bar{W}(\xi,\eta,\zeta) \end{cases}. \tag{18}$$

Finally, we define

$$\begin{cases} \bar{p}(\xi,\eta,\zeta) &= p(-\xi,-\eta,\zeta) \\ \bar{\rho}(\xi,\eta,\zeta) &= \rho(-\xi,-\eta,\zeta) \\ \bar{e}(\xi,\eta,\zeta) &= e(-\xi,-\eta,\zeta) \end{cases}. \tag{19}$$

Using definitions (17), (19) and equation (18) in equation (16) yields the original Euler equations, in which each variable has been replaced by its barred counterpart. The boundary conditions also remain unchanged, and (2) is a solution of (1), if and only if

$$\bar{\mathbf{q}} = |\mathbf{J}|^{-1}\begin{pmatrix} \bar{\rho} \\ \bar{\rho}\bar{u} \\ \bar{\rho}\bar{v} \\ \bar{\rho}\bar{w} \\ \bar{e} \end{pmatrix} \tag{20}$$

also satisfies (1). A necessary condition for uniqueness is that the solution of (1) satisfies the symmetry conditions

$$\begin{cases} \rho(\xi,\eta,\zeta) &= \rho(-\xi,-\eta,\zeta) \\ u(\xi,\eta,\zeta) &= -u(-\xi,-\eta,\zeta) \\ v(\xi,\eta,\zeta) &= -v(-\xi,-\eta,\zeta) \\ w(\xi,\eta,\zeta) &= w(-\xi,-\eta,\zeta) \\ e(\xi,\eta,\zeta) &= e(-\xi,-\eta,\zeta) \end{cases}. \tag{21}$$

The following proposition has been proved:

**Proposition 2.1** *Suppose data satisfies (21). Then, if there is a solution to (1) for which the symmetry condition (21) does not hold, this solution cannot be unique.*

# 3 Artificial viscosity

We have chosen a finite difference method with explicit time-stepping. Centered spatial difference operators are used in the interior and one-sided operators at the boundaries. Nonlinear phenomena, such as shocks and aliasing, cause numerical instabilities. To remedy this situation numerical dissipation is introduced. It is created through a fourth-order difference term (in $\mathbf{q}$), which is turned off near shocks so as not to cause any spurious effects. At shocks we use a second-order difference to filter the solution. In this section we consider three different dissipation operators at and near the boundary: a positive definite operator [8], a semidefinite operator [3], and an indefinite operator. The operators only differ in the treatment of the boundary, and can be represented by matrices of a bandwidth determined by the difference operator in the interior of the domain. We consider three different factorizations of the semidefinite operator, in addition to the unfactored operator. The different factorizations yield dissipation operators with different stability properties.

## 3.1 Interior Points

The semidiscrete Euler equations for a time independent geometry, including artificial viscosity, are

$$\frac{\partial \check{\mathbf{q}}_{jkl}}{\partial \tau} = |\mathbf{J}_{jkl}|[D_0^\xi \mathbf{F}_{jkl} + D_0^\eta \mathbf{G}_{jkl} + D_0^\zeta \mathbf{H}_{jkl} - D_{AV}\check{\mathbf{q}}_{jkl}], \tag{22}$$

where

$$\begin{cases} \mathbf{F}_{jkl} &= \mathbf{F}(\mathbf{q}_{jkl}) \\ \mathbf{G}_{jkl} &= \mathbf{G}(\mathbf{q}_{jkl}) \\ \mathbf{H}_{jkl} &= \mathbf{H}(\mathbf{q}_{jkl}) \end{cases}.$$

The discrete difference operators $D_0^\xi, \Delta_+^\xi$ and $\Delta_-^\xi$ are defined by

$$\begin{cases} D_0^\xi \phi_{jkl} &= (\phi_{j+1,kl} - \phi_{j-1,kl})/(2\Delta\xi) \\ \Delta_+^\xi \phi_{jkl} &= \phi_{j+1,kl} - \phi_{jkl} \\ \Delta_-^\xi \phi_{jkl} &= \phi_{jkl} - \phi_{j-1,kl} \end{cases} . \tag{23}$$

The remaining operators are defined analogously. Furthermore, we assume a time independent geometry for which

$$\Delta\xi = \Delta\eta = \Delta\zeta = 1.$$

The complete coordinate transformation will be discussed in detail in section 3.3. The following formulations of $D_{AV}\check{\mathbf{q}}_{jkl}$ have been proposed [4, 3, 8]:

$$\begin{aligned} D_{AV}\check{\mathbf{q}}_{jkl} &= |\mathbf{J}_{jkl}|^{-1}\sigma_{jkl}\varepsilon^\xi[\Delta_+^\xi\Delta_-^\xi]^2\check{\mathbf{q}}_{jkl} \\ &+ |\mathbf{J}_{jkl}|^{-1}\sigma_{jkl}\varepsilon^\eta[\Delta_+^\eta\Delta_-^\eta]^2\check{\mathbf{q}}_{jkl} \\ &+ |\mathbf{J}_{jkl}|^{-1}\sigma_{jkl}\varepsilon^\zeta[\Delta_+^\zeta\Delta_-^\zeta]^2\check{\mathbf{q}}_{jkl} \end{aligned} \tag{24}$$

$$\begin{aligned} D_{AV}\check{\mathbf{q}}_{jkl} &= \Delta_-^\xi[|\mathbf{J}_{jkl}|^{-1}\sigma_{jkl}\varepsilon^\xi\Delta_+^\xi\Delta_-^\xi\Delta_+^\xi\check{\mathbf{q}}_{jkl}] \\ &+ \Delta_-^\eta[|\mathbf{J}_{jkl}|^{-1}\sigma_{jkl}\varepsilon^\eta\Delta_+^\eta\Delta_-^\eta\Delta_+^\eta\check{\mathbf{q}}_{jkl}] \\ &+ \Delta_-^\zeta[|\mathbf{J}_{jkl}|^{-1}\sigma_{jkl}\varepsilon^\zeta\Delta_+^\zeta\Delta_-^\zeta\Delta_+^\zeta\check{\mathbf{q}}_{jkl}] \end{aligned} \tag{25}$$

$$\begin{aligned} D_{AV}\check{\mathbf{q}}_{jkl} &= \Delta_-^\xi\Delta_+^\xi[|\mathbf{J}_{jkl}|^{-1}\sigma_{jkl}\varepsilon^\xi\Delta_-^\xi\Delta_+^\xi\check{\mathbf{q}}_{jkl}] \\ &+ \Delta_-^\eta\Delta_+^\eta[|\mathbf{J}_{jkl}|^{-1}\sigma_{jkl}\varepsilon^\eta\Delta_-^\eta\Delta_+^\eta\check{\mathbf{q}}_{jkl}] \\ &+ \Delta_-^\zeta\Delta_+^\zeta[|\mathbf{J}_{jkl}|^{-1}\sigma_{jkl}\varepsilon^\zeta\Delta_-^\zeta\Delta_+^\zeta\check{\mathbf{q}}_{jkl}], \end{aligned} \tag{26}$$

where

$$\check{\mathbf{q}}_{jkl} = |\mathbf{J}_{jkl}|\mathbf{q}_{jkl} \tag{27}$$

$$\begin{aligned} \sigma_{jkl} &= |U_{jkl}| + |V_{jkl}| + |W_{jkl}| \\ &+ a_{jkl}(|\nabla\xi_{jkl}|_2 + |\nabla\eta_{jkl}|_2 + |\nabla\zeta_{jkl}|_2) \end{aligned} \tag{28}$$

$$\varepsilon^\xi = \varepsilon^\eta = \varepsilon^\zeta = \vartheta_4 \tag{29}$$

with no smoothing at shocks. The constant $\vartheta_4$ has a value of approximately 0.01. For a better treatment of shocks we add one of the following quantities to $D_{AV}\check{\mathbf{q}}_{jkl}$:

$$\begin{aligned} D_{SH}\check{\mathbf{q}}_{jkl} &= -|\mathbf{J}_{jkl}|^{-1}\sigma_{jkl}\epsilon_{jkl}^\xi\Delta_+^\xi\Delta_-^\xi\check{\mathbf{q}}_{jkl} \\ &-|\mathbf{J}_{jkl}|^{-1}\sigma_{jkl}\epsilon_{jkl}^\eta\Delta_+^\eta\Delta_-^\eta\check{\mathbf{q}}_{jkl} \\ &-|\mathbf{J}_{jkl}|^{-1}\sigma_{jkl}\epsilon_{jkl}^\zeta\Delta_+^\zeta\Delta_-^\zeta\check{\mathbf{q}}_{jkl} \end{aligned} \tag{30}$$

or the conservative variant

$$\begin{aligned} D_{SH}\check{\mathbf{q}}_{jkl} &= -\Delta_-^\xi[|\mathbf{J}_{jkl}|^{-1}\sigma_{jkl}\epsilon_{jkl}^\xi\Delta_+^\xi\check{\mathbf{q}}_{jkl}] \\ &-\Delta_-^\eta[|\mathbf{J}_{jkl}|^{-1}\sigma_{jkl}\epsilon_{jkl}^\eta\Delta_+^\eta\check{\mathbf{q}}_{jkl}] \\ &-\Delta_-^\zeta[|\mathbf{J}_{jkl}|^{-1}\sigma_{jkl}\epsilon_{jkl}^\zeta\Delta_+^\zeta\check{\mathbf{q}}_{jkl}]. \end{aligned} \tag{31}$$

The coefficient in front of the difference operator in the $\xi$-direction is given by

$$\epsilon_{jkl}^\xi = \vartheta_2 \max(\Upsilon_{j+l,kl}^\xi, \Upsilon_{jkl}^\xi, \Upsilon_{j-1,kl}^\xi) \tag{32}$$

with

$$\Upsilon_{jkl}^\xi = \frac{|p_{j+1,kl} - 2p_{jkl} + p_{j-1,kl}|}{|p_{j+1,kl} + 2p_{jkl} + p_{j-1,kl}|}. \tag{33}$$

A typical value of the constant $\vartheta_2$ is 1/4. The other coefficients are defined analogously. The max-function is used to increase the second-order dissipation coefficients near the shock. The fourth-order coefficients

$$\varepsilon^\xi, \quad \varepsilon^\eta, \quad \varepsilon^\zeta$$

can no longer be treated as constants. Instead we set

$$\begin{aligned} \varepsilon^\xi &= \varepsilon_{jkl}^\xi &&= \max(0, \vartheta_4 - \epsilon_{jkl}^\xi) \\ \varepsilon^\eta &= \varepsilon_{jkl}^\eta &&= \max(0, \vartheta_4 - \epsilon_{jkl}^\eta) \\ \varepsilon^\zeta &= \varepsilon_{jkl}^\zeta &&= \max(0, \vartheta_4 - \epsilon_{jkl}^\zeta). \end{aligned} \tag{34}$$

Near shocks the pressure gradients are very strong, causing the max-function to switch off the fourth-order dissipation.

## 3.2 Boundary Points

In this section we define and determine the conservation properties and null spaces of the dissipation operator proposed by Eriksson [3], a positive definite operator [8] and an unsymmetric operator. The only difference between the three dissipation operators is in the handling of the boundaries. Furthermore, we also derive three different factorizations of the operator due to Eriksson.

A simple analysis of the discrete fourth-order dissipation can be based on the equation

$$\frac{\partial\phi}{\partial\tau} = \mathbf{D}_4\phi, \tag{35}$$

where $\mathbf{D}_4$ is the matrix representation of the dissipation operator. To see if $\mathbf{D}_4$ is moment preserving in time, we study the equation

$$\frac{\partial Q_p}{\partial\tau} = \sum_{j=0}^{j=N} j^p \frac{\partial\phi_j}{\partial\tau} = \sum_{j=0}^{j=N} j^p D_4\phi_j, \tag{36}$$

where $D_4$ is a fourth-order *scalar* operator, and $Q_p$ is the $p$-th order moment defined by [3]

$$Q_p = \sum_{j=0}^{j=N} j^p\phi_j, \qquad p \geq 0. \tag{37}$$

We use the notation $D_4$ for fourth-order operators at interior points as well as boundary points. The last equality in equation (36) follows from (35). We will determine the null space of the dissipation operators, and whether or not the dissipation operators are definite.

### 3.2.1 A positive semidefinite fourth-order dissipation operator.

Denote by $[\Delta_+\Delta_-]^2$ the fourth-order operator in any direction. Applying this operator to an interior point yields

$$[\Delta_+\Delta_-]^2\phi_j = \phi_{j-2} - 4\phi_{j-1} + 6\phi_j - 4\phi_{j+1} + \phi_{j+2}. \tag{38}$$

Eriksson [3] has shown that for periodic boundary conditions this operator is positive semidefinite, preserves zeroth, first, second and third order moments, i.e., that equation (36) vanishes identically for $p = 0, 1, 2, 3$, and that the null space consists of all polynomials of degree less or equal to three.

With the boundary conditions we consider, the fourth-order dissipation operators cannot be used as presented in section 3.1. Eriksson has suggested a procedure for specifying the boundary operators such that the total operator (including the boundary modifications) inherits as many of the properties as possible of the operator in the interior with periodic boundary conditions.

With respect to uniformity of the computations and communications in a data parallel implementation, it is desirable that the dissipation operators in matrix form have constant bandwidth. We adopt the convention that $0^0 = 1$. Thus, we need not treat the zeroth moment separately. The most general form of the fourth-order dissipation operator, subject to the constant bandwidth constraint, is

$$\mathbf{D}_4 = \begin{pmatrix} \alpha_0 & \alpha_1 & \alpha_2 & & & & \\ \beta_0 & \beta_1 & \beta_2 & \beta_3 & & & \\ 1 & -4 & 6 & -4 & 1 & & \\ & \ddots & \ddots & \ddots & \ddots & \ddots & \\ & & 1 & -4 & 6 & -4 & 1 \\ & & & \gamma_{N-3} & \gamma_{N-2} & \gamma_{N-1} & \gamma_N \\ & & & & \delta_{N-2} & \delta_{N-1} & \delta_N \end{pmatrix}, \tag{39}$$

since we want to recover the operator given by (38) for a grid function with compact support. Carrying out the summation over $j$ in equation (36) and rearranging the terms yields

$$\frac{\partial Q_p}{\partial \tau} = \sum_{j=0}^{N} \lambda_j \phi_j, \tag{40}$$

where $\lambda_j = [\Delta_+\Delta_-]^2 j^p$ for $j = 4 \ldots N-4$. The coefficients in front of $\phi_2, \phi_3, \phi_{N-3}$ and $\phi_{N-2}$ become fourth-order differences if

$$\begin{aligned} \alpha_2 = \beta_3 = \gamma_{N-3} = \delta_{N-2} = 1 \\ \beta_2 = \gamma_{N-2} = -4. \end{aligned}$$

Clearly, this choice is optimal for moment preservation, since $\phi_j[\Delta_+\Delta_-]^2 j^p$ vanishes at all interior points whenever $p \leq 3$. As for the boundaries, moments of order exceeding one cannot be preserved, since there are only two unknowns in each stencil, with the stencils containing three and four points, respectively. Preserving the zeroth and first order moments yields

$$\begin{aligned} \alpha_0 = \delta_N = 1 \\ \alpha_1 = \delta_{N-1} = \gamma_N = \beta_0 = -2 \\ \beta_1 = \gamma_{N-1} = 5, \end{aligned}$$

or

$$\mathbf{D}_4 = \begin{pmatrix} 1 & -2 & 1 & & & & \\ -2 & 5 & -4 & 1 & & & \\ 1 & -4 & 6 & -4 & 1 & & \\ & \ddots & \ddots & \ddots & \ddots & \ddots & \\ & & 1 & -4 & 6 & -4 & 1 \\ & & & 1 & -4 & 5 & -2 \\ & & & & 1 & -2 & 1 \end{pmatrix}. \tag{41}$$

The null space of the interior operator is obviously a polynomial of degree less or equal to three. To show this property the recurrence relation (38) is solved for a homogeneous right hand side. For the solution to belong to the null space of the boundary operators, the third and second order terms must vanish identically. Hence the null space of $\mathbf{D}_4$ consists of polynomials of degree less or equal to one, the best possible with three point boundary stencils. Finally [3]

$$\phi^T \mathbf{D}_4 \phi = \sum_{j=1}^{N-1} [\Delta_+\Delta_-\phi_j]^2 \geq 0.$$

This inequality holds for the operator defined by (38) as well. Hence, the boundary operator is also semidefinite. We have shown that moments of order $p \leq 1$ are preserved. Increasing $p$ implies the introduction of zeros in the first and last column, making the operator indefinite (in any energy norm). Similarly, increasing the null space dimension of (39) implies a loss of semidefiniteness. With respect to moments, null space dimension, and definiteness the operator (41) is optimum.

**Proposition 3.1** *With respect to moments, null space dimension and definiteness the optimal restriction of (38) to a finite grid with non-periodic boundary conditions is given by (41).*

### 3.2.2 A positive definite fourth-order dissipation operator.

To see how a positive definite dissipation operator affects the rate of convergence we introduce the following operator (see also [8]):

$$\tilde{\mathbf{D}}_4 = \begin{pmatrix} 5 & -4 & 1 & & & & \\ -4 & 6 & -4 & 1 & & & \\ 1 & -4 & 6 & -4 & 1 & & \\ & \ddots & \ddots & \ddots & \ddots & \ddots & \\ & & 1 & -4 & 6 & -4 & 1 \\ & & & 1 & -4 & 6 & -4 \\ & & & & 1 & -4 & 5 \end{pmatrix}. \tag{42}$$

This operator is obtained by deleting the first and last rows and columns of (41). This is equivalent to prescribing Dirichlet boundary conditions.

**Proposition 3.2** *The symmetric operator $\tilde{\mathbf{D}}_4$ defined by equation (42) is positive definite, i.e., it preserves no moments and its null space consists of only the null vector.*

**Proof**
By straightforward arithmetic

$$\phi^T \tilde{\mathbf{D}}_4 \phi = [2\phi_0 - \phi_1]^2 + \sum_{j=1}^{N-1} [\Delta_+\Delta_-\phi_j]^2 + [2\phi_N - \phi_{N-1}]^2 \geq 0.$$

Hence, the operator is positive semi-definite. If $\phi^T \tilde{\mathbf{D}}_4 \phi = 0$, then each term must equal zero, and

$$\phi_{j+2} - 2\phi_{j+1} + \phi_j = 0,$$

which has the solution $\phi_j = \alpha + \beta j$, where $\alpha$ and $\beta$ are determined by the boundary conditions such that

$$\begin{cases} \phi_1 &= 2\phi_0 \\ \phi_{N-1} &= 2\phi_N \end{cases}$$

are satisfied, or

$$\begin{pmatrix} -1 & 1 \\ -1 & -N-1 \end{pmatrix} \begin{pmatrix} \alpha \\ \beta \end{pmatrix} = \begin{pmatrix} 0 \\ 0 \end{pmatrix}.$$

Since $N$ must be a positive integer, $\alpha = \beta = 0$. Thus $\phi_j = 0, j = 0, \ldots N \iff \phi = 0$. Hence, $\tilde{\mathbf{D}}_4$ is positive definite. Since the column sum of the first column is different from zero, the operator cannot preserve any moment. As $\tilde{\mathbf{D}}_4$ is positive definite, it follows that zero cannot be an eigenvalue of (42); thus the only member of the null space is the null vector. □

### 3.2.3 An indefinite, unsymmetric, fourth-order dissipation operator.

We also consider the non-symmetric fourth-order dissipation operator

$$\bar{\mathbf{D}}_4 = \begin{pmatrix} 0 & 0 & 0 & & & & \\ -1 & 3 & -3 & 1 & & & \\ 1 & -4 & 6 & -4 & 1 & & \\ & \ddots & \ddots & \ddots & \ddots & \ddots & \\ & & 1 & -4 & 6 & -4 & 1 \\ & & & 1 & -3 & 3 & -1 \\ & & & & 0 & 0 & 0 \end{pmatrix}. \quad (43)$$

Polynomials of degree less or equal to two constitute the null space of (43). Only zeroth order moments are preserved ([3] or use equation (40)). Since the first diagonal entry is zero, (43) is indefinite.

### 3.2.4 Conservative and non-conservative dissipation operators.

The conservation property of the analytic Euler equations should be inherited by the numerical scheme, especially for shock computations. Clearly, the operators (41) and (43) are conservative (each row can be thought of as a first difference of something else). The operator (42) is *not* conservative at the boundary point and at the first interior point. All the operators are preceded by adaptive scaling factors (see (25)). Since the scaling factors depend upon the mesh size as well as the solution itself, the conservation property of the operators (41), (42) and (43) may be lost at *every* point. Furthermore, the definiteness property may also be lost. But, as will be shown in the next section, the adaptive scaling can be incorporated such that the dissipation operator is both conservative and positive semidefinite.

### 3.2.5 Factorization of the symmetric, positive semidefinite dissipation operator.

The dissipation operator $\mathbf{D}_4$ can be factored as

$$\mathbf{D}_4 = \mathbf{D}_1^- \mathbf{D}_3^+,$$

where

$$\mathbf{D}_1^- = \begin{pmatrix} 1 & & & & & & \\ -1 & 1 & & & & & \\ & -1 & 1 & & & & \\ & & \ddots & \ddots & & & \\ & & & -1 & 1 & & \\ & & & & -1 & 1 & \\ & & & & & -1 & 1 \end{pmatrix} \quad (44)$$

$$\mathbf{D}_3^+ = \begin{pmatrix} 1 & -2 & 1 & & & & \\ -1 & 3 & -3 & 1 & & & \\ & -1 & 3 & -3 & 1 & & \\ & & \ddots & \ddots & \ddots & \ddots & \\ & & & -1 & 3 & -3 & 1 \\ & & & & -1 & 2 & -1 \\ & & & & & 0 & 0 \end{pmatrix} \quad (45)$$

The total artificial viscosity operator (in one space dimension) is

$$\mathbf{D}_1^- \Sigma \mathbf{D}_3^+, \quad (46)$$

where

$$\Sigma = \mathrm{diag}(\varepsilon_0 \sigma_0 |\mathbf{J}_0|^{-1}, \ldots, \varepsilon_N \sigma_N |\mathbf{J}_N|^{-1}).$$

Here $\sigma_j$, $\varepsilon_j$ and $|\mathbf{J}_j|^{-1}$ are the one-dimensional equivalents of (29), (34) and (4), respectively. Obviously, the operator is conservative.

This factorization corresponds to splitting the fourth-order operator $[\Delta_-\Delta_+]^2$ into $\Delta_-$ and $\Delta_+\Delta_-\Delta_+$. Since $\Delta_+$ and $\Delta_-$ commute, an alternative splitting is $\Delta_+$ and $\Delta_-\Delta_+\Delta_-$. To facilitate the formal manipulation of the matrix representation we use the equivalent splitting $-\Delta_+$ and $-\Delta_-\Delta_+\Delta_+$. In matrix notation

$$\mathbf{D}_4 = \mathbf{D}_1^+ \mathbf{D}_3^-,$$

where

$$\mathbf{D}_1^+ = \begin{pmatrix} 1 & -1 & & & & & \\ & 1 & -1 & & & & \\ & & 1 & -1 & & & \\ & & & \ddots & \ddots & & \\ & & & & 1 & -1 & \\ & & & & & 1 & -1 \\ & & & & & & 1 \end{pmatrix} \quad (47)$$

$$\mathbf{D}_3^- = \begin{pmatrix} 0 & 0 & & & & & \\ -1 & 2 & -1 & & & & \\ 1 & -3 & 3 & -1 & & & \\ & \ddots & \ddots & \ddots & \ddots & & \\ & & 1 & -3 & 3 & -1 & \\ & & & 1 & -3 & 3 & -1 \\ & & & & 1 & -2 & 1 \end{pmatrix} \quad (48)$$

Note that $\mathbf{D}_1^{+T} = \mathbf{D}_1^-$. Using the factorization $\mathbf{D}_4 = \mathbf{D}_1^+ \mathbf{D}_3^-$, the dissipation operator is defined as

$$\mathbf{D}_1^+ \Sigma \mathbf{D}_3^- \quad (49)$$

which also is conservative. Moreover,

$$\mathbf{D}_4 = \mathbf{D}_1^- \mathbf{D}_1^+ \mathbf{D}_2 = \mathbf{D}_1^+ \mathbf{D}_1^- \mathbf{D}_2, \quad (50)$$

where

$$\mathbf{D}_2 = \begin{pmatrix} 0 & 0 & & & \\ -1 & 2 & -1 & & \\ & \ddots & \ddots & \ddots & \\ & & -1 & 2 & -1 \\ & & & 0 & 0 \end{pmatrix}. \qquad (51)$$

This factorization yields the following fourth-order dissipation operator

$$\mathbf{D}_1^- \mathbf{D}_1^+ \Sigma \mathbf{D}_2 \qquad (52)$$

which satisfies [3]

$$\phi^T \mathbf{D}_1^- \mathbf{D}_1^+ \Sigma \mathbf{D}_2 \phi = \sum_{j=1}^{N-1} \sigma_j \varepsilon_j |\mathbf{J}_j|^{-1} [\Delta_+ \Delta_- \phi_j]^2.$$

Hence, this operator is positive semidefinite. It preserves the zeroth and first order moments, and its null space is all polynomials of degree less or equal to one. The analysis of $\mathbf{D}_1^- \Sigma \mathbf{D}_3^+$ and $\mathbf{D}_1^+ \Sigma \mathbf{D}_3^-$ is more involved and will not be carried out here. The operators have different stability properties. Consider

$$\begin{aligned} \phi^T \mathbf{D}_1^- \Sigma \mathbf{D}_3^+ \phi &= (\mathbf{D}_1^- \Sigma \mathbf{D}_1^+ \phi)^T \mathbf{D}_2 \phi \\ \phi^T \mathbf{D}_1^+ \Sigma \mathbf{D}_3^- \phi &= (\mathbf{D}_1^+ \Sigma \mathbf{D}_1^- \phi)^T \mathbf{D}_2 \phi, \end{aligned}$$

where

$$\mathbf{D}_1^- \Sigma \mathbf{D}_1^+ \phi \neq \mathbf{D}_1^+ \Sigma \mathbf{D}_1^- \phi$$

The first choice yields a stable scheme, whereas the second choice is unstable. The factorization in (52) is the preferred choice. Table 1 summarizes the properties of the dissipation operators.

| Dissipation Operator | Definiteness | Preservation of Moments | Dimension of Null Space |
|---|---|---|---|
| $\mathbf{D}_4$ | positive semidefinite | $\leq$ first order | 2 |
| $\tilde{\mathbf{D}}_4$ | positive definite | none | 0 |
| $\bar{\mathbf{D}}_4$ | indefinite | zeroth order | 3 |
| $\mathbf{D}_1^- \Sigma \mathbf{D}_3^+$ | | | 2 |
| $\mathbf{D}_1^+ \Sigma \mathbf{D}_3^-$ | | | 2 |
| $\mathbf{D}_1^- \mathbf{D}_1^+ \Sigma \mathbf{D}_2$ | positive semidefinite | $\leq$ first order | 2 |

Table 1: Properties of the Dissipation Operators

## 3.3 Spatial Discretization

We have chosen a transformation between the physical and computational grids such that $\Delta\xi = \Delta\eta = \Delta\zeta = 1$, the origin of the physical coordinates coincides with the center of the channel cross-section at the inflow boundary, and the range of the computational coordinates is $0 \leq \xi_j \leq N_\xi$, $0 \leq \eta_k \leq N_\eta$ and $0 \leq \zeta_l \leq N_\zeta$. Denote the cross-sectional physical side lengths by $L_x$ and $L_y$, and the physical channel length by $L_z$. The complete transformation between the computational and the physical grids $(\xi, \eta, \zeta) \rightarrow (x, y, z)$ is

$$\begin{cases} x &= \xi' \cos(\omega(\zeta)/N_\zeta) &- \eta' \sin(\omega(\zeta)/N_\zeta) \\ y &= \xi' \sin(\omega(\zeta)/N_\zeta) &+ \eta' \cos(\omega(\zeta)/N_\zeta) \\ z &= \zeta L_z / N_\zeta \end{cases}, \qquad (53)$$

where

$$\begin{cases} \xi' &= (2\xi/N_\xi - 1)\, L_x/2 \\ \eta' &= (2\eta/N_\eta - 1)\, L_y/2 \end{cases} \qquad (54)$$

and

$$\omega(\zeta) = \begin{cases} 0 & \zeta \in [0, \zeta_0) \\ \omega'(\zeta) & \zeta \in [\zeta_0, \zeta_1) \\ \bar{\omega} & \zeta \in [\zeta_1, N_\zeta] \end{cases}. \qquad (55)$$

where $\omega'(\zeta) = \bar{\omega}(3\zeta_1 - \zeta_0 - 2\zeta)(\zeta - \zeta_0)^2 (\zeta_1 - \zeta_0)^{-3}$. Hence, $\omega(\zeta)$ is a $C^1$-spline on the interval $[0, N_\zeta]$. Introducing this spline function enables a $C^1$-grid transformation, which is such that the homogeneous inflow condition $u = 0$, $v = 0$, $w = w_0$, where $u$, $v$ and $w$ denote the Cartesian velocity components, yields continuous velocity gradients even at the inflow boundary. The function $\omega(\zeta)$ describes how the twisting factor (angular frequency) increases from 0 to $\bar{\omega}$ along the $\zeta$-axis, which coincides with the physical $z$-axis. We use

$$\bar{\omega} = 2\pi / N_\zeta.$$

All the metric coefficients are derived from (53), (54), (55) and

$$\mathbf{J}'' = \begin{pmatrix} \xi_x & \xi_y & \xi_z \\ \eta_x & \eta_y & \eta_z \\ \zeta_x & \zeta_y & \zeta_z \end{pmatrix} = \begin{pmatrix} x_\xi & x_\eta & x_\zeta \\ y_\xi & y_\eta & y_\zeta \\ z_\xi & z_\eta & z_\zeta \end{pmatrix}^{-1}. \qquad (56)$$

## 3.4 Time Discretization

A three stage Runge-Kutta method is used to integrate the semidiscrete Euler equations in time. It belongs to a class of integration methods that can be written

$$\begin{cases} \check{\mathbf{q}}_{jkl}^0 &= \check{\mathbf{q}}_{jkl}^n \\ \check{\mathbf{q}}_{jkl}^1 &= \check{\mathbf{q}}_{jkl}^0 + \alpha_1 \Delta\tau \mathbf{R}(\check{\mathbf{q}}_{jkl}^0) \\ &\vdots \\ \check{\mathbf{q}}_{jkl}^m &= \check{\mathbf{q}}_{jkl}^0 + \alpha_m \Delta\tau \mathbf{R}(\check{\mathbf{q}}_{jkl}^{m-1}) \\ \check{\mathbf{q}}_{jkl}^{n+1} &= \check{\mathbf{q}}_{jkl}^m \end{cases}. \qquad (57)$$

The vector $\mathbf{R}$ is the right member of equation (22). For a three stage Runge-Kutta method $m = 3$. The steady solution is independent of the coefficients $\alpha_j$ and $\Delta\tau$. This property also holds if $\Delta\tau$ is replaced by a local time step $\Delta\tau_{jkl}^n$. The coefficients $\alpha_j$ can be looked upon as acceleration parameters [2]. We have used $\alpha_1 = \alpha_2 = \alpha_3 = 1$. The local time step is computed as [7]

$$\Delta\tau \leq \frac{CFL}{|U| + |V| + |W| + a(|\nabla\xi|_2 + |\nabla\eta|_2 + |\nabla\zeta|_2)} \equiv \frac{CFL}{\sigma}, \qquad (58)$$

where the definition of $\sigma$ in (58) is the same as in (29). The Courant-Friedrichs-Lewy number, or $CFL$ number, equals 1.27.

## 3.5 Numerical Methods, Summary

In summary, the Euler flow equations are based on the twisted grid as defined by equations (53), (54) and (55), and the semidiscrete equations

$$\begin{aligned}\frac{\partial \check{\mathbf{q}}_{jkl}}{\partial \tau} &= |\mathbf{J}_{jkl}|[D_0^\xi \mathbf{F}_{jkl} + D_0^\eta \mathbf{G}_{jkl} + D_0^\zeta \mathbf{H}_{jkl}] \\ &- \sigma_{jkl}\varepsilon^\xi_{jkl}[\Delta^\xi_+\Delta^\xi_-]^2\check{\mathbf{q}}_{jkl} \\ &- \sigma_{jkl}\varepsilon^\eta_{jkl}[\Delta^\eta_+\Delta^\eta_-]^2\check{\mathbf{q}}_{jkl} \\ &- \sigma_{jkl}\varepsilon^\zeta_{jkl}[\Delta^\zeta_+\Delta^\zeta_-]^2\check{\mathbf{q}}_{jkl} \\ &+ \sigma_{jkl}\epsilon^\xi_{jkl}\Delta^\xi_+\Delta^\xi_-\check{\mathbf{q}}_{jkl} \\ &+ \sigma_{jkl}\epsilon^\eta_{jkl}\Delta^\eta_+\Delta^\eta_-\check{\mathbf{q}}_{jkl} \\ &+ \sigma_{jkl}\epsilon^\zeta_{jkl}\Delta^\zeta_+\Delta^\zeta_-\check{\mathbf{q}}_{jkl}\end{aligned} \tag{59}$$

in non-conservative form and

$$\begin{aligned}\frac{\partial \check{\mathbf{q}}_{jkl}}{\partial \tau} &= |\mathbf{J}_{jkl}|\{D_0^\xi \mathbf{F}_{jkl} + D_0^\eta \mathbf{G}_{jkl} + D_0^\zeta \mathbf{H}_{jkl} \\ &- \Delta^\xi_-[|\mathbf{J}_{jkl}|^{-1}\sigma_{jkl}\varepsilon^\xi_{jkl}\Delta^\xi_+\Delta^\xi_-\Delta^\xi_+\check{\mathbf{q}}_{jkl}] \\ &- \Delta^\eta_-[|\mathbf{J}_{jkl}|^{-1}\sigma_{jkl}\varepsilon^\eta_{jkl}\Delta^\eta_+\Delta^\eta_-\Delta^\eta_+\check{\mathbf{q}}_{jkl}] \\ &- \Delta^\zeta_-[|\mathbf{J}_{jkl}|^{-1}\sigma_{jkl}\varepsilon^\zeta_{jkl}\Delta^\zeta_+\Delta^\zeta_-\Delta^\zeta_+\check{\mathbf{q}}_{jkl}] \\ &+ \Delta^\xi_-[|\mathbf{J}_{jkl}|^{-1}\sigma_{jkl}\epsilon^\xi_{jkl}\Delta^\xi_+\check{\mathbf{q}}_{jkl}] \\ &+ \Delta^\eta_-[|\mathbf{J}_{jkl}|^{-1}\sigma_{jkl}\epsilon^\eta_{jkl}\Delta^\eta_+\check{\mathbf{q}}_{jkl}] \\ &+ \Delta^\zeta_-[|\mathbf{J}_{jkl}|^{-1}\sigma_{jkl}\epsilon^\zeta_{jkl}\Delta^\zeta_+\check{\mathbf{q}}_{jkl}]\}\end{aligned} \tag{60}$$

or

$$\begin{aligned}\frac{\partial \check{\mathbf{q}}_{jkl}}{\partial \tau} &= |\mathbf{J}_{jkl}|\{D_0^\xi \mathbf{F}_{jkl} + D_0^\eta \mathbf{G}_{jkl} + D_0^\zeta \mathbf{H}_{jkl} \\ &- \Delta^\xi_-\Delta^\xi_+[|\mathbf{J}_{jkl}|^{-1}\sigma_{jkl}\varepsilon^\xi_{jkl}\Delta^\xi_-\Delta^\xi_+\check{\mathbf{q}}_{jkl}] \\ &- \Delta^\eta_-\Delta^\eta_+[|\mathbf{J}_{jkl}|^{-1}\sigma_{jkl}\varepsilon^\eta_{jkl}\Delta^\eta_-\Delta^\eta_+\check{\mathbf{q}}_{jkl}] \\ &- \Delta^\zeta_-\Delta^\zeta_+[|\mathbf{J}_{jkl}|^{-1}\sigma_{jkl}\varepsilon^\zeta_{jkl}\Delta^\zeta_-\Delta^\zeta_+\check{\mathbf{q}}_{jkl}] \\ &+ \Delta^\xi_-[|\mathbf{J}_{jkl}|^{-1}\sigma_{jkl}\epsilon^\xi_{jkl}\Delta^\xi_+\check{\mathbf{q}}_{jkl}] \\ &+ \Delta^\eta_-[|\mathbf{J}_{jkl}|^{-1}\sigma_{jkl}\epsilon^\eta_{jkl}\Delta^\eta_+\check{\mathbf{q}}_{jkl}] \\ &+ \Delta^\zeta_-[|\mathbf{J}_{jkl}|^{-1}\sigma_{jkl}\epsilon^\zeta_{jkl}\Delta^\zeta_+\check{\mathbf{q}}_{jkl}]\}\end{aligned} \tag{61}$$

in conservative form. Equation (61) has not yet been implemented. The reciprocal cell volume at point $jkl$ is computed from equation (3), $\mathbf{F}_{jkl}$, $\mathbf{G}_{jkl}$ and $\mathbf{H}_{jkl}$ are given by equations (6), (7) and (8). The vector $\check{\mathbf{q}}_{jkl}$ is given by equation (27), $\sigma_{jkl}$ by equation (29), $\varepsilon_{jkl}$ by equation (34), $\epsilon_{jkl}$ by equation (32), and the difference operators for interior and boundary points are given by equation (23). For boundary points higher order difference operators are modified as defined by one of equations (41), (42) or (43) and by (51). For the conservative form the fourth-order operator is modified according to equations (44) and (45). The in/outflow boundary conditions are stated at the end of section 2. At the solid boundaries the normal component of the velocity field is zero.

# 4 Simulation results

The effects on the entropy distribution, the flow, and the convergence rate of the different dissipation operators for the Euler equations were studied for a twisted channel of rectangular cross section. The channel dimensions were $0.035 \times 0.0175 \times 0.140\ m^3$. The grid sizes ranged from $32 \times 32 \times 32$ to $32 \times 32 \times 64$, with the total number of grid points ranging from 32,768 to 65,536 points. The demonstrated performance for a fully configured Connection Machine system model CM–2 is 1.1 Gflops/s in single-precision.

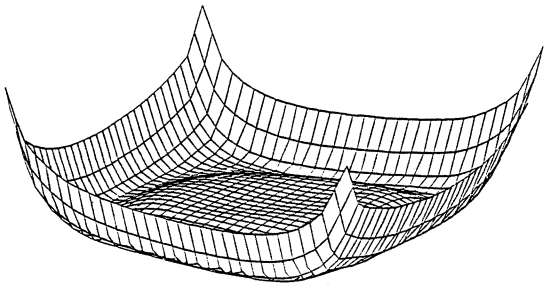

Figure 2: Entropy Distribution at Outflow Boundary, Operator $\tilde{\mathbf{D}}_4$

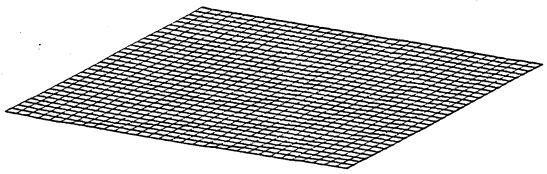

Figure 3: Entropy Distribution at Outflow Boundary, Operator $\mathbf{D}_1^-\Sigma\mathbf{D}_3^+$

Since no shocks are present, the flow must be isentropic throughout the channel, provided that inflow data is isentropic. We compute the entropy as

$$S = c_v \log\left[\frac{p}{(\gamma-1)\rho^\gamma}\right], \tag{62}$$

which is valid for a polytropic gas [1]. Hence, prescribing constant pressure and density at the inflow boundary ensures that the inflow data is isentropic.

Figure 2 and Table 2 show how the entropy piles up at the solid walls for the operator $\tilde{\mathbf{D}}_4$. The entropy distribution for the operator $\mathbf{D}_1^-\Sigma\mathbf{D}_3^+$ is shown in Figure 3. The scale is the same in both figures. Table 2 also shows that $\bar{\mathbf{D}}_4$ and $\mathbf{D}_4$ are entropy preserving.

An indication of the sensitivity of the dissipation operators to perturbations in the inflow data can be obtained from observations of $w$ at the outflow. We studied two cases: completely irrotational inflow, and an inflow with a slight rotation. For the irrotational flow the normalized inflow data is $u = 0$, $v = 0$ and $w = 1$. In the second test case $u \neq 0$ and $v \neq 0$, but small, at the solid walls of the inlet. All interior points at the inflow boundary are the same as for the irrotational case. From the contour plots it is apparent that the choice of dissipation operator *does* affect the flow,

even if the operator is entropy preserving. Comparing the perturbed and the non-perturbed flows, we note that the conservative operator $\mathbf{D}_1^- \Sigma \mathbf{D}_3^+$ appears to be more stable than the non-conservative operators $\mathbf{D}_4$ and $\bar{\mathbf{D}}_4$. In fact, Figures 6 and 9 indicate that $\bar{\mathbf{D}}_4$ not is very robust. Notice also that in Figures 8 and 11 the contour lines are unsymmetric at the corners. The operator $\mathbf{D}_1^- \mathbf{D}_1^+ \Sigma \mathbf{D}_2$ does not have this behavior.

The convergence rate of the operator $\mathbf{D}_1^- \Sigma \mathbf{D}_3^+$ is the highest, Figures 4 and 5. Note the significant change of the convergence rate for the operator $\tilde{\mathbf{D}}_4$ for the irrotational flow, and for the operators $\mathbf{D}_4$ and $\bar{\mathbf{D}}_4$ for the perturbed flow. The change in convergence rate occurs after about 3,000 iterations in the first case, and about 1,500 iterations in the second case. There is also a decrease in the rate of convergence of the operator $\mathbf{D}_1^- \Sigma \mathbf{D}_3^+$ for irrotational flows at about 1,500 iterations. The convergence rate decreases by almost a factor of two. The convergence properties are summarized in Table 3.

| Dissipation operator | Vorticity at inflow boundary | Entropy $S_{\min}$ | Entropy $S_{\max}$ |
|---|---|---|---|
| $\tilde{\mathbf{D}}_4$ | No | 43.64 | 57.57 |
| | Yes | 43.56 | 57.68 |
| $\bar{\mathbf{D}}_4$ | No | 46.67 | 46.86 |
| | Yes | 46.62 | 46.74 |
| $\mathbf{D}_4$ | No | 46.68 | 46.78 |
| | Yes | 46.58 | 46.73 |
| $\mathbf{D}_1^- \Sigma \mathbf{D}_3^+$ | No | 46.76 | 46.94 |
| | Yes | 46.73 | 46.84 |

Table 2: Entropy at Outflow Boundary

| Dissipation operator | Vorticity at inflow boundary | Number of iterations | Residual |
|---|---|---|---|
| $\tilde{\mathbf{D}}_4$ | No | 3900 | 5.8E-6 |
| | Yes | 3900 | 6.8E-6 |
| $\bar{\mathbf{D}}_4$ | No | 5800 | 6.6E-6 |
| | Yes | 5400 | 6.6E-6 |
| $\mathbf{D}_4$ | No | 3900 | 5.8E-6 |
| | Yes | 5400 | 6.9E-6 |
| $\mathbf{D}_1^- \Sigma \mathbf{D}_3^+$ | No | 3400 | 6.5E-6 |
| | Yes | 2800 | 6.7E-6 |

Table 3: Number of Iterations for the Dissipation Operators

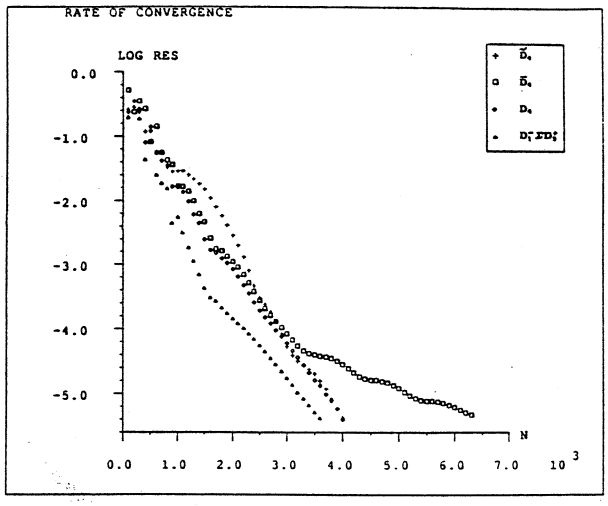


Figure 4: Rate of Convergence for the Different Dissipation Operators, Irrotational Inflow

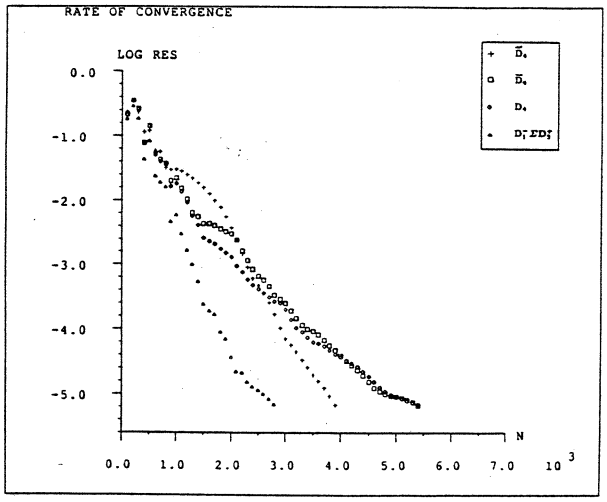


Figure 5: Rate of Convergence for the Different Dissipation Operators, Weakly Rotational Inflow

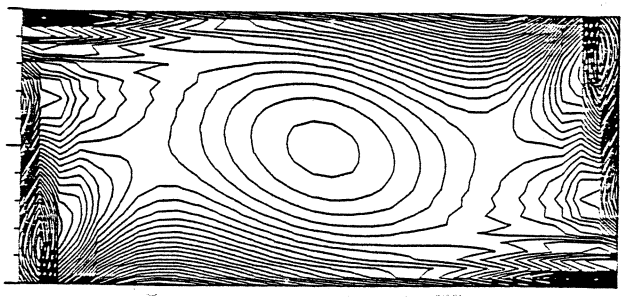

Figure 6: Contour Lines of $w$-component at Outflow, Operator $\tilde{\mathbf{D}}_4$, Irrotational Inflow

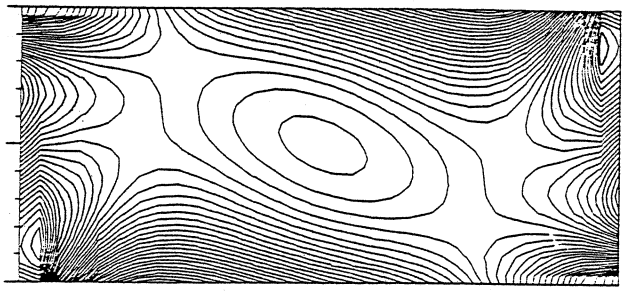

Figure 7: Contour Lines of $w$-component at Outflow, Operator $\mathbf{D}_4$, Irrotational Inflow

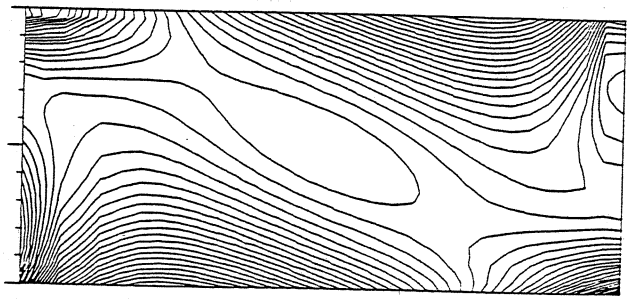

Figure 8: Contour Lines of $w$-component at Outflow, Operator $\mathbf{D}_1^- \Sigma \mathbf{D}_3^+$, Irrotational Inflow

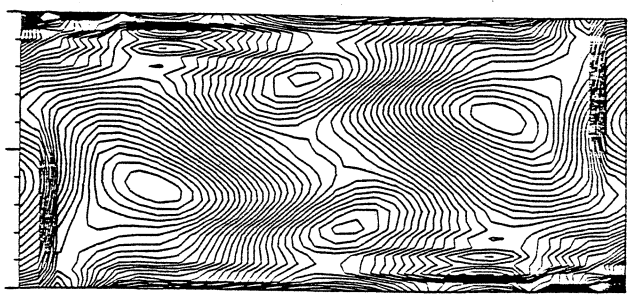

Figure 9: Contour Lines of $w$-component at Outflow, Operator $\tilde{\mathbf{D}}_4$, Weakly Rotational Inflow

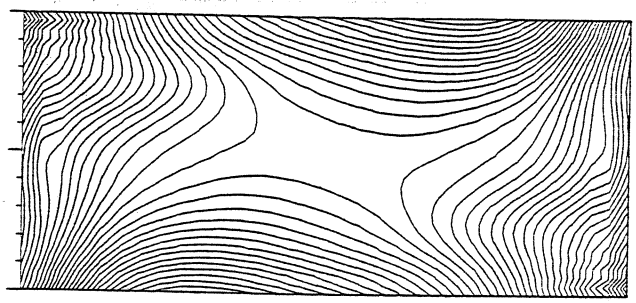

Figure 10: Contour Lines of $w$-component at Outflow, Operator $\mathbf{D}_4$, Weakly Rotational Inflow

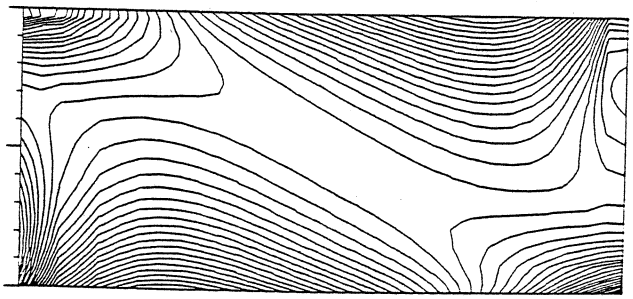

Figure 11: Contour Lines of $w$-component at Outflow, Operator $\mathbf{D}_1^- \Sigma \mathbf{D}_3^+$, Weakly Rotational Inflow

# 5 Summary and Conclusions

We have shown that the non-conservative dissipation operator defined by (42) gives rise to a significant growth in entropy close to the solid walls of the channel, and that the conservative operators do not have this behavior. We have also shown that factorization of the dissipation operator proposed by Eriksson [3] as $\mathbf{D}_1^- \Sigma \mathbf{D}_3^+$ results in a higher rate of convergence than the unfactored operator, both for irrotational and perturbed inflows. The number of iterations for this operator is approximately 90% of those for the dissipation operator defined by (42) in the irrotational case, and approximately 70% in the perturbed case. The stability of the different operators is not the same. The operator $\mathbf{D}_1^- \Sigma \mathbf{D}_3^+$ appears to be most stable, whereas the operator $\bar{\mathbf{D}}_4$ does not seem to be robust.

The finite difference, explicit time stepping algorithm, parallelizes easily and perfectly. A performance of 135 Mflops/s was obtained on a 8,192 processor Connection Machine system model CM–2. The demonstrated performance for a fully configured system of 65,536 processors is 1.1 Gflops/s.


### Acknowledgement

Many thanks are due Bertil Gustafsson for valuable suggestions and critique throughout the project, and for many comments on the manuscript. This project was partially sponsored by The Swedish Board of Technical Development (STU), reg-no 61008767, by Jacob Letterstedts fond, The Royal Swedish Academy of Sciences, and by the Office of Naval Research under Contract No. N00014-86-K-0310. The first implementation of the Euler solver was made in Release 4 of the Connection Machine software. Porting of the program to Release 5 was made by Louis Howell and David Serafini of Thinking Machines Corporation.


# References


[1] R. Courant and K. O. Friedrichs. *Supersonic Flow and Shock Waves*, volume I of *Pure and Applied Mathematics*. Interscience Publishers, Inc., New York, 1948.

[2] Rickard Enander and Johan Sowa. Numerical simulation of fluid flow in a twisted channel. Technical Report 88-01, Department of Scientific Computing, Uppsala University, 1988.

[3] L. E. Eriksson. Boundary conditions for artificial dissipation operators. Technical Report FFA TN 1984-53, The Aeronautical Research Institute of Sweden, Aerodynamics Department, Stockholm, Sweden, 1984.

[4] A. Jameson, W. Schmidt, and E. Turkel. Numerical solutions of the Euler equations by finite volume methods using Runge-Kutta time-stepping schemes. *AIAA Paper*, 81-1259, 1981.

[5] S. Lennart Johnsson. Future high performance computation: The megaflop per dollar alternative. Technical Report YALEU/DCS/RR-360, Dept. of Computer Science, Yale University, January 1985.

[6] Pelle Olsson and S. Lennart Johnsson. A dataparallel implementation of explicit methods for the three-dimensional compressible Navier-Stokes equations. Technical Report CS-89/4, Thinking Machines Corp., February 1989.

[7] Pelle Olsson and S. Lennart Johnsson. A study of dissipation operators for the Euler equations and three-dimensional channel flow. Technical Report CS-89/3, Thinking Machines Corp., February 1989.

[8] Thomas E Pulliam. Artificial dissipation models for the Euler equations. *AIAA*, 24(12), December 1986.